Earth Science Informatics (2025) 18:219
https://doi.org/10.1007/s12145-025-01721-3

RESEARCH

Optimizing rain-gauge network design for enhanced estimate rainfall in ungauged plain and mountainous regions

Mahdi Zarei[1] · **Rasoul Sarvestan**[2] · **Seyed Hassan Alavinia**[3]

Received: 6 November 2024 / Accepted: 16 January 2025

Abstract

Nowadays, due to the insufficient number of stations for input in hydrological models, it is not possible to simulate runoff and floods for points without stations. Therefore, to solve this problem, rain gauge networks should be designed for these station points. The present study was carried out to design an optimal rain gauge network for estimating rainfall in plain and mountainous areas with an area of 39 square kilometers in northeastern Iran. The R software was utilized to identify extreme events within the study area. Four events (representing all of the identified events) were selected and modeled using the weather research and forecasting model under four schemes, namely Purdue-Lin (Lin), WRF Single-Moment class 3,5 (WSM3, WSM5), and WRF Double-Moment class 6 (WDM6). According to the modeling result, 91 rain gauge stations were required to cover the study area, with the rain gauge stations designed at different distances from the synoptic station. The microphysical Lin scheme produced better accuracy levels for the rainfall modeling, as indicated by false alarm ratio and threat score of 17 and 0.91 for the rain-gauge stations located in the mountainous areas and 9 and 0.83 for the rain-gauge stations located in the plain areas, respectively. The rain-gauge stations in the mountainous and plain areas tend to give more acceptable accuracies within 6 and 8 km of the main synoptic station, respectively, as indicated by the False Alarm Ratio (FAR) of 0.30 and 0, respectively. Generally, Outputs of the rain-gauge network design coupled with future-period (24 h) forecasts enable authorities to become aware of extreme rainfall events, and the rainfall data derived from this network can be used as input to hydrological models in non-gauged regions.

Keywords Modeling · Extreme rainfall · WRF · Non-gauged areas · Northeastern Iran

Introduction

Estimation of average rainfall in a watershed based on the measured data at multiple rain-gauge networks plays a crucial role in many hydrological applications (Bastin et al. 1984; Chua and Bras 1982; Shafiei et al. 2014) Rain-gauge networks are used for estimating region-wide average rainfall, spatial diversity, and point rainfall at watershed/urban scale, and most importantly, providing the required inputs for hydrologic and hydraulic modeling (Coustau et al. 2015; Habets et al. 2008; Raimonet et al. 2017; Soci et al. 2016). A rain-gauge network gives high-accuracy rainfall measurements at particular points. In many cases, however, the distribution of the rain-gauge stations is so inappropriate that they cannot represent the spatial and temporal variabilities of the rainfall systems properly (Astin 1997; Villarini et al. 2008). Application of radars and meteorological satellites has become a common approach to rainfall estimation and rain-gauge network building (Krajewski and

Communicated by: Hassan Babaie

✉ Rasoul Sarvestan
r.sarvestan@gmail.com

Mahdi Zarei
m.zarei@hsu.ac.ir

Seyed Hassan Alavinia
s.h.alavinia@kashanu.ac.ir

[1] Research Center of Social Studies & Geographical Sciences, Hakim Sabzevari University, Sabzevar, Iran

[2] Department of Climatology, Faculty of Geography and Environmental Sciences, Hakim Sabzevari University, Sabzevar, Iran

[3] Department of Natural Engineering, Faculty of Natural Resources and Earth Sciences, University of Kashan, Kashan, Iran

Published online: 31 January 2025

Smith 2002; Maddox et al. 2002; Morin et al. 2006; Volkmann et al. 2010; Yatheendradas et al. 2008). Radar/satellite-based estimations, however, suffer from limitations in representing fundamental processes, poor parameterization, and inaccurate measurement instruments, leading to a sort of uncertainties and biases in the outputs (Krajewski and Smith 2002; Smith et al. 1996; Villarini et al. 2008; Volkmann et al. 2010; Young et al. 1999). This holds especially true for small watersheds in mountainous areas where estimating storm depth and severity from the radar data is more challenging than that for flat areas. Therefore, it is not clear to what extent can radar/satellite-based rainfall estimations provide the requirements for accurate rainfall and flood forecasts (Volkmann et al. 2010; Yatheendradas et al. 2008).

To address this gap, it has been recommended to use numerical weather forecast (NWP) models, which are known to offer high accuracy at regional and small watershed/urban scales. The weather research and forecasting (WRF) model represents a modern generation of mid-scale systems for numerical weather forecast, which satisfies not only the weather research needs but also operational forecast demands (Das et al. 2020; Kuznetsova et al. 2019; Skamarock et al. 2005). Accordingly, numerous research has examined the certainty and efficiency of this model in different locations around the world. For instance, Merino et al. (2021) in the Ebro basin on the northeastern Iberian Peninsula (Spain) focused on the precise validation of rainfall networks based on four factors: i.e. station density used to build the network, spatial separation of the network, station height and weather type. For this purpose, 18 grids were constructed using six spatial resolutions and three station densities. The results showed that the density of stations was identified as a major factor, while the spatial resolution of the network was of minor importance. However, the second factor becomes more relevant in regions with strong altitudinal gradients and when high station densities are available. In addition, the weak and moderate precipitation is overestimated in the daily grids. In contrast, heavy precipitation cells are less available, which reduces the variability of the data. In contrast, monthly and annual totals have less deviation from the observed distribution than daily comparisons. Morsy et al. (2021) coupled the products of the GPM satellite with the so-called kriging method for four rainfall events. Based on their study analysis, 31 of the existing rain-gauge stations were confirmed considering the regional height. More recently, Mahoutchi and Abbasi (2021) performed research in Iran where they investigated various configurations of the WRF model to simulate the five-day rainfall events in March and April 2019 in Golestan Province, which demonstrated that the WRF model turned out to overestimate the rainfall at most of the stations. Moreover, the configuration of precipitation cores was well demonstrated and the model performed accurately when it came to rainfall levels.

In most recent studies around the world (China, South Korea, India, Thailand, Spain, Germany, Poland, Greece, and Iran), rainfall estimation and rain-gauge network design have been practiced by applying the spatial techniques across extended basins and river watersheds (Adhikary et al. 2015; Ayanwale and Alabi 2017; Hong et al. 2007; Hou 2018; Jung et al. 2014; Kreklow et al. 2019; Putthividhya and Tanaka 2012; Tian et al. 2018; Tiwari et al. 2020; Usowicz et al. 2021; Xu et al. 2017). These studies have further used remote-sensing (RS) data to determine the distribution of rain-gauge stations across extended basins. Therefore, the present study attempts to use outputs of regional models (e.g., WRF model), instead of large-scale RS data, for small basins (Basins without stations). Numerous studies (Patel et al. 2019; Davis et al. 2022, Castorina et al. 2022) have evaluated the accuracy of the WRF model for the direct forecast of floods. Indeed, using the proposed methodology, one can not only define virtual rain-gauge stations in tough mountainous areas, where the cost of installing and maintaining an actual rain-gauge station is too high but also identify these rain-gauge stations and introduce their numerical data into hydrological and hydraulic models to enable 24-hr rainfall forecast. Being aware of the possible occurrence of a flood event at such points helps urban managers and planners better manage the flood risk and alleviate its consequences and losses. In this study, we try to estimate a suitable rain gauge station network using the Weather Research and Forecasting model for the study area where this problem exists. This causes the uncertainties in hydrological studies to decrease and the accuracy of the studies to increase.

Materials and methods

Study area and data set

The study area is located in the northwest of Khorasan Razavi Province delineated by 36° 9′ 7″ and 36° 22′ 30″ northern latitude and 57°37′30″ and 57°46′10″ eastern longitude, with an average height of 970 from mean sea level. It is limited to Ghuchan, Esfarayen, and Bojnourd to the north, Neyshabour to the east, Kashmar to the south, and Shahroud (Semnan Province) to the west. According to De Martonne aridity index, the study area is dominated by an arid climate. Figure 1 shows the location map of the study area. The studied area is divided into six sub-basins: Sabzevar, Joyn, Ataieh, Qala Maidan, Derune and Davarzen. The largest area of this region belongs to the Sabzevar sub-basin. The total length of the rivers in this area is 2,897.5 km, with the longest river measuring 27.63 km. The elevation of various basins ranges from 756 to 2,944 m, with the highest

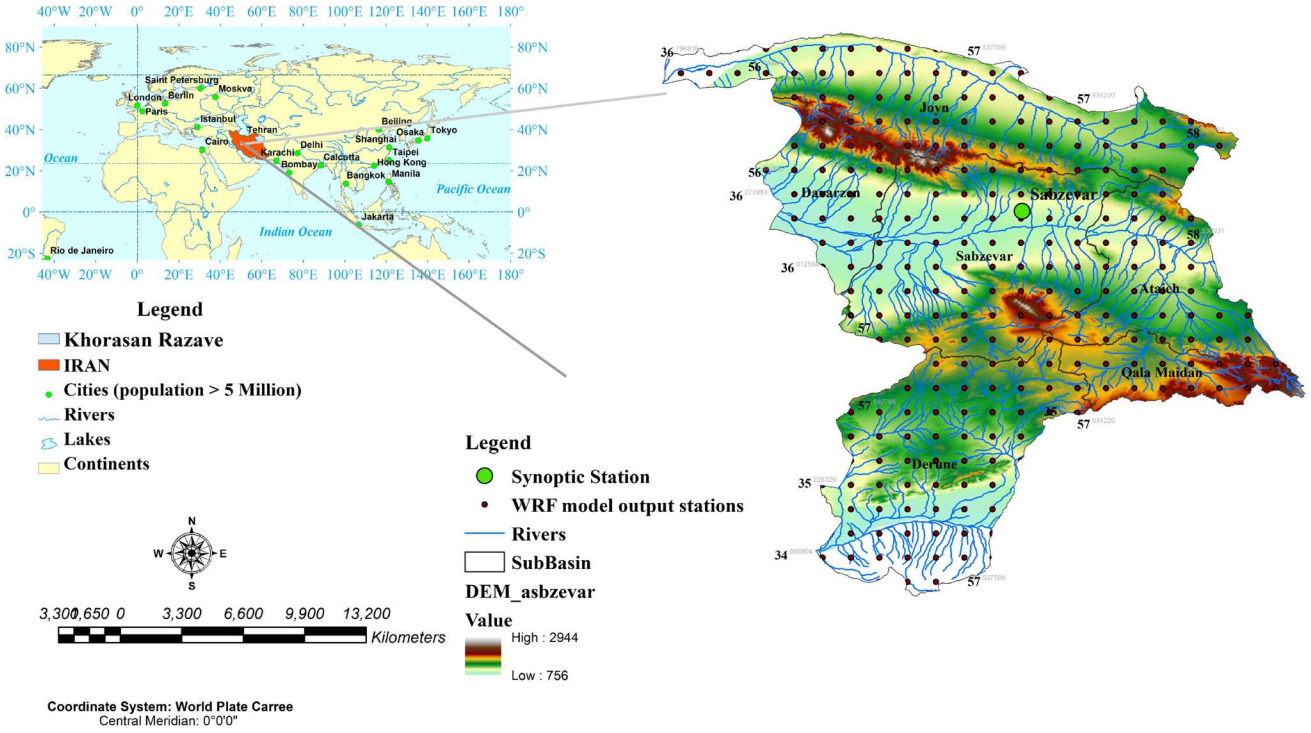

Fig. 1 The geographical location of the case study

elevations falling between 1,500 and 1,900 m. The average rainfall for 40 years is 320 mm per year. The volume of precipitation and surface water are 1895.1 and 13.6 million cubic meters per year, respectively Of this volume of rainfall, 1780.2 million cubic meters per year evaporate and transpire (Statistical yearbook 2019). In the winter season, the distribution of rainfall reaches its maximum and reaches zero during the summer. The highest amount of rainfall in the statistical period was related to February, with 38 mm, and the lowest amount was related to the month of September, with 0.03 mm. The maximum daily rainfall was in May, which was 12 mm per day (Iran Meteorological Office. Due to the geographical location of the region and its hot, dry climate, it is exposed to heavy rains every year, which causes many human and financial losses. Also, the location of the studied area is in a dry climate, and the lack of rainwater infiltration causes rainfall to cover all parts of human life and the surrounding environment in a short period. Due to these cases, the weakest amount of precipitation can also be selected as a precipitation event for the region.

Once the extreme rainfall events at the studied station were identified, all events covering such rainfall levels were extracted as representative of the extreme events, as listed in Table 1.

In this table, we first identified extreme rainfall based on the values of the statistical period 1961 to 2021. Then, based on these extreme rainfalls, 4 recent events were identified

Table 1 Selected events and approved thresholds in rainfall modeling in both mountainous and plain areas (authors)

Row	Extreme events (mm/day) 1961–2021	Recent selected events (mm/day)	
1	1	2019/29/10	1
2	5	2020/10/01	5
3	10	2019/18/03	10
4	39	2020/04/11	36

that are representative of the climate of the study area (their values are close to extreme rainfalls).

These events were then modeled with the WRF model under different schemes Purdue-Lin (Lin), WRF Single-Moment class 3,5 (WSM3, WSM5), and WRF Double-Moment class 6 (WDM6) to evaluate the accuracy of different schemes for non-gauged areas in the mountains and plains. Findings for different schemes are detailed in the following.

The data used in this research come in two main categories: observational data and Global Forecast System (GFS) data. The GFS is a numerical weather forecast system operated by the US National Weather Service (NWS). GFS forecast products at 0.25° × 0.25° resolution are obtained from the National Center for Atmospheric Research (NCAR) Research Data Archive (RDA) Historical GFS Archive

(NCEP 2015). The GFS runs four times daily at 0000, 0600, 1200, and 1800 UTC. These data are available in pgrb2, pgrb2b and pgrb2full formats. One of the output variables of the GFS model is accumulated rainfall, where the rainfall forecasts are the accumulations starting from the time the model was run (Yue et al. 2022). GFS data are the input data that the WRF model uses to forecast or simulate events. These data are taken from the website 24 h before each event. The specifications of these data are given in the table.

Rainfall observation data for the selected period of 60 years (1961 to 2021) was received from the Iran Meteorological Organization. Out of the entire dataset, four recent events (2019–2021) representing extreme rainfall, wet seasons, and all rainfall levels from low to moderate and high were selected. Developed at the National Centers for Environmental Prediction (NCEP), GFS is a weather forecast model that provides data for several meteorological and land variables, including temperature, wind, rainfall, soil moisture, ozone concentration, etc. This system adjoins four independent models (i.e., atmosphere, ocean, earth/soil and sea ice models), which work together to draw an accurate image of weather conditions. Specifications of the data used in this research are given in Table 2.

Methodology

Model configuration

The RClimDex software was used to prepare the meteorological data in order to extract the rainfall limit profiles. Zhang and Yang developed this software at the Climatic Research Branch of the Meteorological Service of Canada. The National Development Agency of Canada initially developed it through the Canada-China Climate Change Cooperation Project. This software is based on calculating extreme profiles of climatic parameters (Fortin et al. 2017; Mohammadi et al. 2017; Zhang and Yang 2004) (Fortin et al. 2017; Mohammadi et al. 2017; Zhang and Yang 2004). But in this research, it is only used for the limit rainfall profile.

In this research, the RClimDex software was used only to classify the rainfall thresholds of the studied area. In fact, by classifying the rainfall of the study area, the amount of the maximum rainfall is identified, and according to the rainfall values, the threshold of the events is determined. To control the quality of data in this method, we compared the obtained rainfall threshold value with observed rainfall values, and the accuracy of the threshold of considered limit rains was obtained (Table 3).

After determining these limit profiles, to be able to make the best rainfall forecasts on the Sabzevar urban basin in the future. Therefore, the selection of events must follow both of the following factors (Rodrigo et al. 2018).

a) have a cover of maximum rainfall according to the rainy and low rainfall seasons of the year.
b) Events that first correspond to heavy rainfall at the station level should be selected.

The advanced research model of WRF is a three-dimensional primary equation meteorological circulation model widely used to predict rainfall events (Rodrigo et al. 2018). To model extreme rainfall events, we used the Advanced Research Version of the Weather Research and Forecasting Model (WRF 4.1.5) run under Linux and with the Bash programming language. This model is also used in operational weather forecasting and research studies. (used at NCEP and other national meteorological centers as well as in real-time forecasting configurations at laboratories, universities, and companies.). In the present research, the WRF-ARW model was configured on a Mercator map design to demonstrate the study area along with the surrounding arid areas with a particular center.

The configuration was done for a longitude range of 57.01–58.65°E, a latitude range of 35.12–36.17°N, and a nested domain including an outer and an inner domain of 9 and 5 km in resolution, respectively with grid cells of 9×9 km in dimensions. With a resolution of $0.25° \times 0.25°$, initial and boundary conditions were interpolated from GFS by NCEP. The boundary and initial conditions for the inner domain were produced from the output fields of the outer domain by the model itself. Extreme events that occurred on June 31st, 2020, December 31st, 2019, February 7th, 2021, and March 24th, 2020 were modeled since 25-hr ahead of the event on UTC basis. The modeling was focused on 24-hr rainfall periods ending at UTC 00, resembling the 24-hr rainfall criterion used by the Iran Meteorological Organization. For the microphysical scheme, the default model uses

Table 2 Global Forecast System (GFS) data feature

Scale/Network(°)	Registration period	Model cycle (UTC)	Formats	Output time (Hours)
0.25°	After 30 Days	00	pgrb2 pgrb2b pgrb2full	0 to 24

Table 3 Rainfall indices recommended by the expert group Commission for Climatology/CLIVAR: climate variability and predictability (CCL / CLIVAR) (Zhang and Yang 2004)

Index number	Definition	Units
Rx1day (1)	Max1day rainfall amount	mm
Rx5day (2)	Max5day rainfall amount	mm
R10mm (3)	Number of heavy rainfall days	day
R39mm (4)	Number of very heavy rainfall days	day

the same configuration as that of the WRF-ARW model used in the Iran Meteorological Organization.

We herein used a microphysical scheme where the Kain-Fritsch cumulus scheme was used for physics (Kain 2004), the YSU scheme was used for planetary boundary layers (PBL), and microphysics schemes of Lin, WSM3, WSM5, and WDM6 (Hong et al. 2004; Hong and Lim 2006; Naing 2021) were used to simulate the inner domain (Lim and Hong 2010). Once events with the two abovementioned (a and b) criteria were identified, an attempt was made to improve the accuracy of the WRF model by checking the results with four different schemes, namely Lin, WSM3, WSM5, and WDM6. The characteristics of each of the different schemas are as follows:

The Lin scheme

The Lin scheme, developed by Lin and colleagues during 1982–1983, incorporates several advanced features for cloud and rainfall modeling: The scheme accounts for ice sedimentation processes, considering the half-life of rainfall particles. It utilizes collision-coalescence and aggregation processes for spontaneous particle transformation. It is capable of simulating rainfall from anvil clouds that do not reach the surface. The scheme adopts the Marshall-Palmer distribution function for particle size distribution (Lin et al. 2008, 2011).

The WSM3 scheme

The WSM3 scheme, developed by Hong, Dudhia, and Chen in 2004, is designed for mesoscale modeling and includes advanced microphysical processes: It considers snow and rain, cloud ice and cloud water, and vapor as its primary components. The scheme accounts for ice formation processes below freezing temperatures. It is particularly suited for mesoscale grids, incorporating ice and snow-related processes. Unlike the Marshall-Palmer distribution, it explicitly represents mixed-phase hydrometeors, such as graupel and hail (Hong et al. 2004; Verlinde et al. 1990).

The WSM5 scheme

The WSM5 scheme, developed by Hong, Dudhia, and Chen in 2004, represents an advanced version of the WSM3 microphysical scheme with expanded capabilities: It incorporates five categories of microphysical processes, including ice. The scheme models sedimentation processes exclusively as ice. Instead of the Marshall-Palmer distribution, it explicitly considers mixed-phase hydrometeors, such as graupel and hail (Hong et al. 2004). It is designed for high-resolution simulations, accounting for processes involving snow, snowflakes, and ice crystals (Liu et al. 2011).

The WDM6 scheme

The WDM6 scheme is an advanced microphysical parameterization that expands upon the WSM6 scheme, incorporating six categories of hydrometeors along with detailed processes: It includes six microphysical components, such as snowflakes, rain, and cloud particles. This scheme extends the WSM6 by employing a two-moment approach to represent warm rain processes, considering both the mass and number concentration of raindrops. It enhances the representation of condensation, cloud density, and rainfall forecasting (Bae et al. 2016).

Based on the geographical and climatic conditions of the study area, which are compatible with these schemes (according to the features of the schemes), and considering the findings of previous research (Sarvestan et al. 2022) conducted in the region, it was determined that these schemes significantly influence the simulation of regional rainfall. Therefore, these schemes were selected for the study to enhance the accuracy of the modeling process. To use dynamic outputs of the WRF model, The Grid Analysis and Display System (GrADS) was used to convert the output data to point information (i.e., establishing a rain-gauge network in non-gauged areas) (Mafas et al. 2016; Rahman 2017). Table 2 lists some of the most important nodes of the rain-gauge network as per outputs of the WRF model upon dividing the network of rain-gauge stations into two parts, namely mountainous and plain rain-gauge stations. In the present research, the certainty and accuracy of forecasting these non-gauged areas were verified through two criteria, namely TS and FAR. Figure 2 shows the main steps of running the meteorological model and designing the proposed station network.

Verification

To study the accuracy of the meteorological model in forecasting the rainfall of the region, it is necessary to compare and evaluate it with verification methods. In these methods, the performance of the meteorological model in forecasting rainfall for each station is calculated by comparing the amount of observed rainfall with the amount of forecasted rainfall. In order to evaluate the accuracy of each of the schemas, The WRF model is run for each event's number of schemas (16 times run). We compare each run with the amount of observed rainfall (Table 4). Its value is evaluated according to the coefficients in Table 5 and the verifications in Table 4, and the best scheme is selected. Finally, conclusions can be drawn by analyzing the quantities mentioned.

Then, calculations will be done with the equations below:

Table 4 Features of several rain gauge station network outputs of the WRF model

Type of stations	No	Network of stations (km)	Altitude	Longitude (E)	Latitude (*N*)
Mountainous	1	13.82	1407	57°69´	36°33
	2	18.78	1523	57°80´	36°33
	3	26.79	1717	57°39	36°33
	4	26.96	1951	57°49	36°41
	5	32.73	2272	57°39	36°41
	6	41.48	1028	58°10	36°15
	7	50.26	1736	58°21	26° 24
	8	14.07	1271	57°29	36°33
	9	19.33	1333	57°49	36°33
	10	31.95	1110	58°00	36°24
Plain	11	5.4	1031	57°69	26°24
	12	6	1022	57°59	36°24
	13	7.66	915	57°69	36°15
	14	8.11	894	57°59	36°15
	15	13.81	1032	57°80	36°24
	16	14.56	994	57°49	36°24
	17	15.55	881	57°49	36°15
	18	16.72	1000	57°69	36°06
	19	16.93	958	57°59	36°06
	20	18.85	938	57°80	36°15

Table 5 A contingency table (2×2) (Kodamana and Fletcher 2021; Mohammadiha et al. 2012; Satya et al. 2021)

		Observed		
		Yes	No	Total
Forecast	Yes	Hits	False Alarms	forecast yes
	No	Misses	Correct Negatives	observed no
	Total	observed yes	observed no	Total

A contingency table is used to see the occurrences of rainfall events

Hits = the event that is predicted to happen actually happened

False Alarm = the predicted event did not occur

Missed = the event that was predicted did not happen, happened

Correct Negatives = Events that were predicted not to occur did not occur

$$Accurayion\ (ACC) = \frac{Hits + correct\ negatives}{Total} \quad (1)$$

$$Threat\ Score\ (TC) = \frac{Hits}{Hits + Misses + False\ Alarms} \quad (2)$$

$$False\ Alarm\ Ratio\ (FAR) = \frac{False\ Alarms}{Hits + False\ Alarms} \quad (3)$$

$$Probability\ of\ Detection\ (POD) = \frac{Hits}{Hits + Misses} \quad (4)$$

The range and best values for REI indicators are shown in Table 6 below (Kodamana and Fletcher 2021; Mohammadiha et al. 2012; Satya et al. 2021).

Results

Extreme rainfall events

In the present research, extreme rainfall events observed at the northeast synoptic station during its entire data recording span (1961–2021) were identified according to 4 extreme indicators (Fig. 3). According to the results, the first indicator (RX 1 day) reflected the maximum 24-hr rainfall, which was 39 mm occurring in 1977, 1982, and 1988. The minimum 24-hr rainfall was 9.6 followed by 9.4 mm, which occurred in 2008 and 2013, respectively. Also, the findings showed that the maximum 24-hour rainfall has a decreasing trend with a slope of −0.048, that the trend is significant, and is the value of P-value = 0.043. The second indicator (RX 5 day) used in this study was the maximum 5-day rainfall. The maximum and minimum 5-day rainfall were seen to be 89.6 and 10.8 mm, which occurred in 2020 and 2008, respectively. Investigations represented a significant (P-value = 0.014) increasing trend whose slope value is 0.186. As the third indicator (R10mm) considered in this study, heavy rainfall (≥ 10 mm) was observed for a maximum of 13, 12, and 11 days, respectively.

This climate profile also has a significant increasing trend (P-value = 0.026) whose slope is 0.024. Based on the results, the heavy rainfall periods, as the third indicator, exhibited an increasing trend with time. The fourth (R 39 mm) and the most extreme rainfall indicator at the northeast synoptic station for the studied period was 39 mm rainfall. According to the obtained results, it can be concluded that 24-hr rainfall reached 39 mm at three events that occurred in 1977, 1982, and 1988. This climatic profile has a significant decreasing trend (P-value = 0.046), whose slope value is −0.001. Rain-gauge network of WRF model.

After validating the meteorological model, its output has been used as a rain gauge station in the region.

Table 6 REI indicator values

REI indicators	Range value	Best value
TS	0–1	1 (max)
ACC	0–1	1 (max)
POD	0–1	1 (max)
FAR	0–1	0 (min)

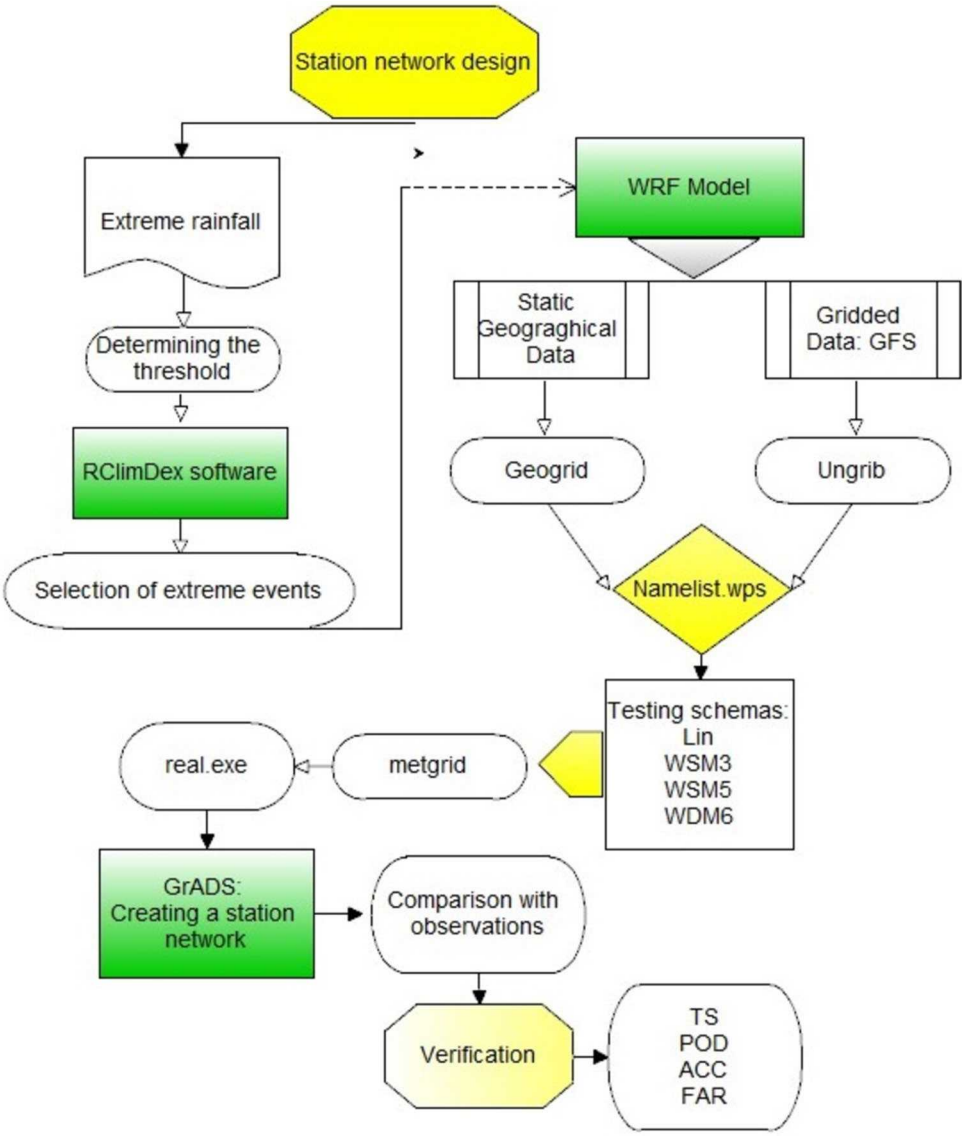

Fig. 2 Flowchart of main steps for Station network design in the present study

To establish a rain gauge network in areas lacking existing stations, an initial attempt was made to utilize the network of stations generated by the meteorological model outputs. However, these stations required optimization. For this purpose, the entire network generated by the WRF model for the study area (Fig. 4a) was used. This network consisted of 270 stations with a spatial resolution of 9×9 km. According to the World Meteorological Organization (WMO), the recommended maximum distance between synoptic stations is approximately 25 km. In this study, to ensure better coverage, the maximum distance from the Sabzevar synoptic station was considered to be twice this standard, i.e., 55 km. Based on this criterion, 91 rain gauge stations were selected around the Sabzevar synoptic station. Subsequently, after comparing the simulated rainfall data with observational data from the Sabzevar station during various events, 27 rain gauge networks were finalized for the region (Fig. 4b).

Microphysical schemes

After the extreme rainfall event in four different scenarios, each time it was run in the WRF model. The numerical output of this model in each of the scenarios was obtained with 27 station points (9×9 km) at a distance of 6.5 km from the Sabzevar synoptic station of these 27 rain gauge stations, 10 stations are located in the mountainous area and 17 points are located in the plains. Figure 4 shows the difference between observed and predicted rainfall levels with different schemes across the rain-gauge network in the mountainous part. In this figure, the blue dotted line is the rainfall threshold (the closer the values are between zero and the blue dotted line, the better the accuracy of the scheme). Investigation of the event that occurred on October 1st, 2020 states that the WSM5 and WSM3 schemes produced more accurate results within 13 and 18 km of the synoptic station,

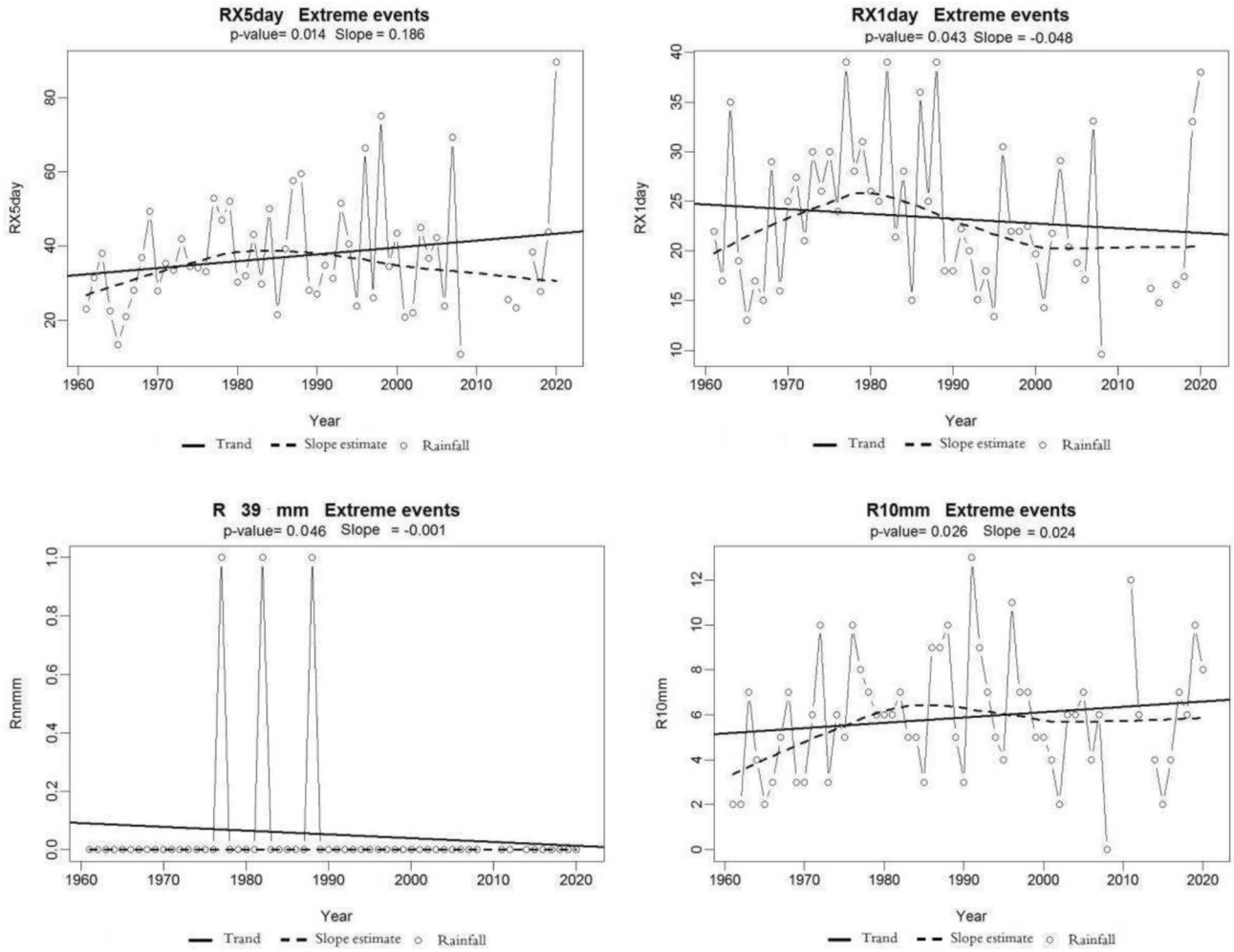

Fig. 3 The status of the rainfall extreme event of the northeast synoptic stations since its establishment (1961–2021)

respectively. As is evident from the rainfall threshold of this event (−1, +1), the selected scheme for the WRF model ended up with significantly different rainfall levels compared to the observational values in this mountainous area (Fig. 5A). Investigation of the extreme event that occurred on April 11th, 2020 for the mountainous rain-gauge network displayed that the Lin scheme can accurately model the rainfall in this area. Further Findings showed that all schemes exhibit similar trends when the considered point gets farther from the synoptic station, with the only difference being the deviation of the modeled values out of observed levels of rainfall, which was larger with WSM3 and WDM6 and smaller with Lin and WSM3 (Fig. 5B). Rainfall modeling for the event that occurred on 29th October 2019 in the mountainous area (Fig. 5C) indicated that similar to other studied events, the Lin scheme exhibited good accuracy and precision in the rainfall modeling across the rain-gauge network in the corresponding areas. Indeed, with this scheme, we could predict rainfall with an average error of 0.2 mm within a distance of 13–21 km to the main synoptic station. In this part, the WSM3 returned the lowest accuracy of rainfall modeling across the network, as indicated by up to 0.67 mm deviation of the modeled values out of observed data. Figure 5D shows rainfall modeling for the event that occurred on 18th March 2019 in the mountainous areas in the west of the study area. Given the rainfall threshold (+3, −3) in this extreme event, the Lin scheme was still the best-performing scheme for rainfall modeling in this area. The average error of rainfall modeling under the Lin scheme, concerning observational data, was found to reach as low as −1.88 mm.

Investigation of the extreme event that occurred on October 1st, 2020 for the rain-gauge stations located in the plain area showed that the Lin scheme provides for higher accuracy. Accordingly, with this scheme, the rainfall deviation reached 0 mm within 7–8 and 15–21 km of the considered synoptic station (Fig. 6A). Investigation of the findings of the rain-gauge network in the plain area for the

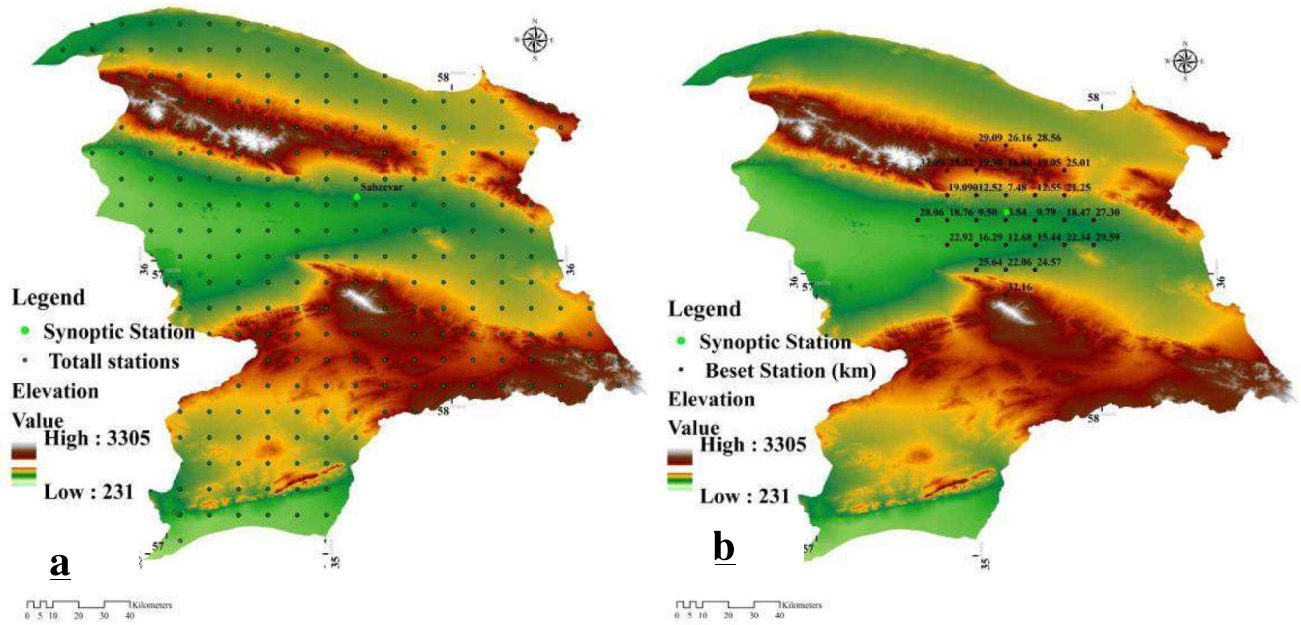

Fig. 4 **a** All of the network output stations of the WRF model, **b** The network of selected stations for evaluation

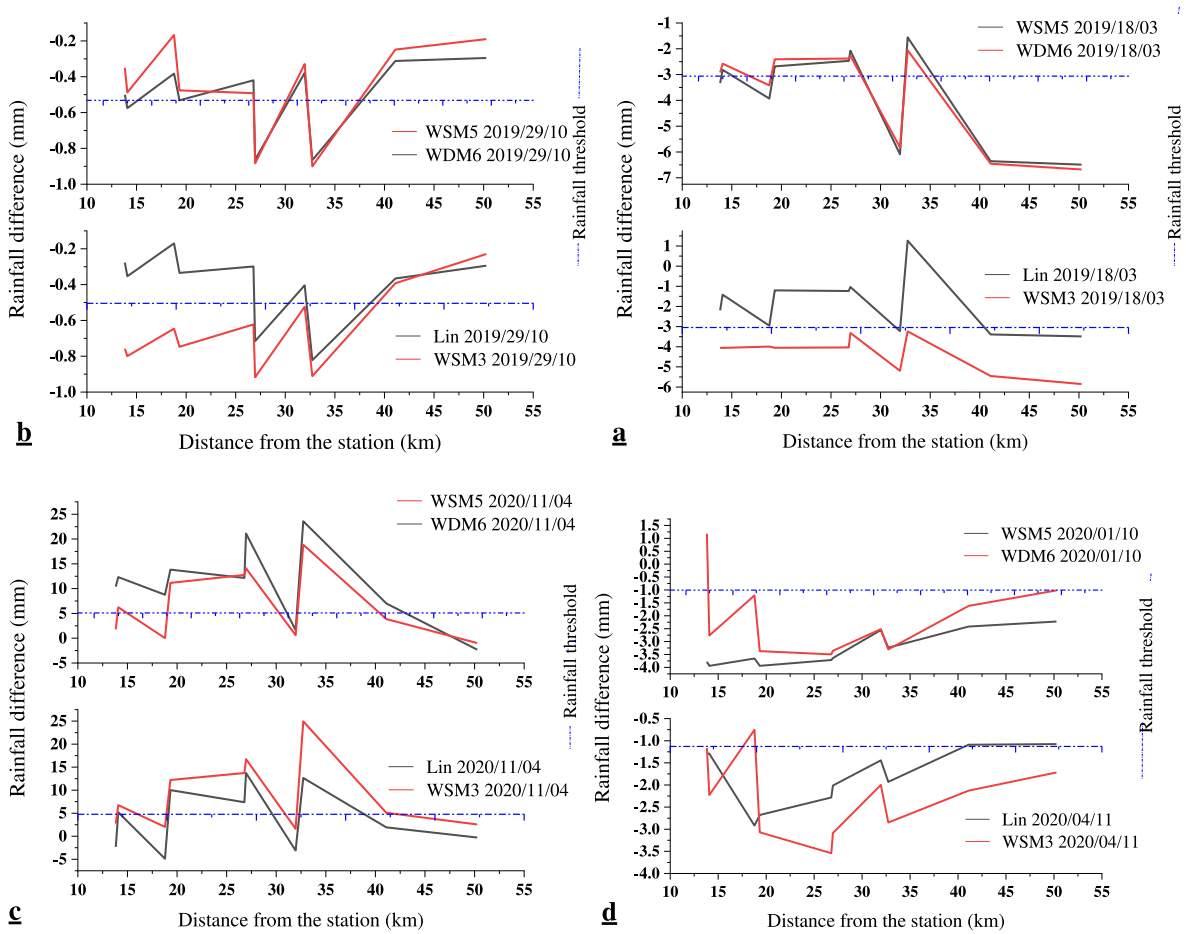

Fig. 5 The difference in rainfall compared to the synoptic station in the network of rain gauge stations located in the mountains of the study area

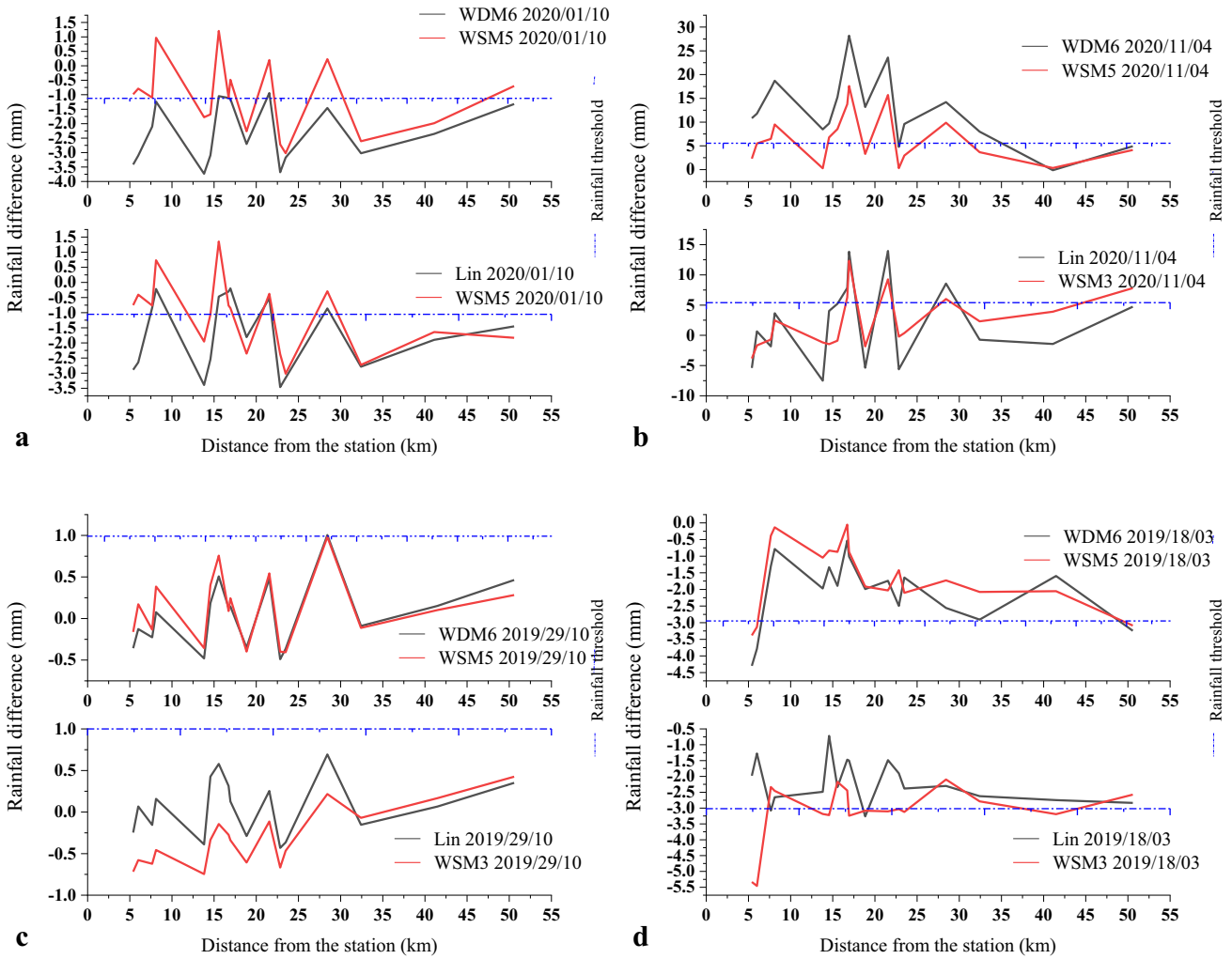

Fig. 6 The difference in rainfall compared to the synoptic station in the network of rain gauge stations located in the plains of the study area

extreme event that occurred on April 11th, 2020 illustrated that the Lin and WSM3 schemes provide for higher power and accuracy in extreme rainfall estimation across the network. The accuracy of these two schemes was even higher in the plain area rather than in the mountainous area. For example, the Lin scheme could model the rainfall with an error of 0.65 mm at a distance of 6 km to the synoptic station, indicating the power and accuracy of this scheme for modeling 24-hr rainfall in this extreme event (Fig. 6B). Investigation of rain-gauge networks located in the western plains of the study area indicates that, among the evaluated schemes, the Lin scheme could model the rainfall with acceptable accuracy. Considering this extreme indicator, the rain-gauge network in this part of the study area was associated with much smaller deviations than the observation data (i.e., as low as 0.5 mm) (Fig. 6C Modeling the extreme event occurred on March 18th, 2020 showed that, for the plain areas in eastern Iran, heavy rainfall (36 mm) can be better modeled with the WRF model with different schemes, with this superior accuracy being evident with the Lin and WSM5 schemes. Deviation of modeled rainfall out of observation data over the rain-gauge network in the plain areas reached an average of −1.59 mm, while the corresponding figure to the WSM5 scheme was −2.17 mm (Fig. 6D).

Validation assessment of the rainfall modeling with the four schemes over the rain-gauge network in the mountainous areas is demonstrated in Fig. 7. In verification processes for positive and negative metrics, the symbols “Y” and “N” have distinct meanings. For positive-oriented metrics, such as TS, ACC and POD, values exceeding 70 are categorized as “Y,” indicating superior scheme performance. Conversely, values below 70 are marked as “N,” reflecting weaker performance. However, for negative-oriented metrics, such as FAR, the interpretation is reversed. Values below 30 are considered “Y,” representing better scheme performance, whereas values exceeding 30 are classified as “N,” indicating poor performance.

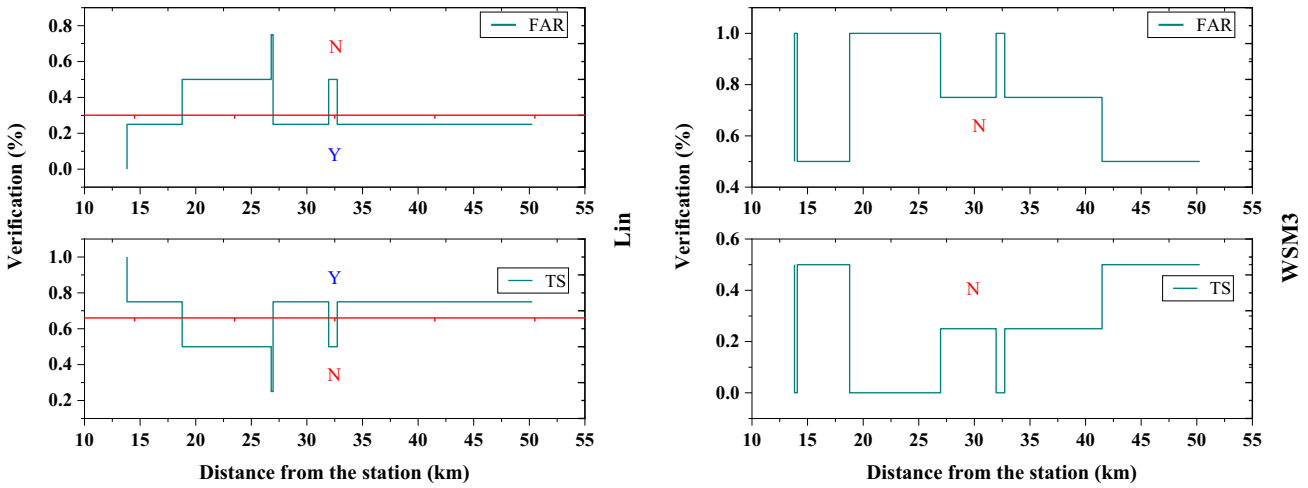

Fig. 7 Comparison of verification of different schemes in the network of rain gauge stations located in mountainous areas (Y: Acceptable, N: Unacceptable)

Evaluated based on the FAR (as a negative point) and TS, POD and ACC (as a positive point), the WSM3 and WDM6 schemes were found to perform very poorly in rainfall modeling in the mentioned areas. Findings further suggested that the Lin scheme provides the highest accuracy for rainfall modeling in the same area so that it generates zero FAR at 5 and 6 km distances to the main synoptic station coupled with TS, POD and ACC levels above 70% at most of the points across the network (Fig. 7).

According to the FAR, TS, POD and ACC verification of the rain-gauge network in the plain area (Fig. 8) states that different schemes of the WRF model exhibit better accuracies in rainfall modeling in plain areas, where most of the rain-gauge network exhibited deviations within the verifiable range. Moreover, the Lin scheme produced zero FAR coupled with unit TS, POD and ACC at all points at a distance of 6–8 or 41–50 km to the synoptic station, indicating the superiority of this scheme over other schemes.

Presenting estimations of average rainfall coupled with spatial diversity and point rainfall at the scale of urban and non-urban watersheds, outputs of the rain-gauge network from the dynamic meteorological model of WRF serve as the most important inputs to hydrological models (Soci et al. 2016). In the present research, the dynamic model of WRF was used to downscale and design a rain-gauge network with a spatial and temporal resolution of 9 km and 1-hr, respectively, to properly cover the study area. Table 7 presents the final status of the designed rain gauge stations based on the outputs of the dynamic model using the strong parameterization scheme. This table is compiled using the best verification method. The closer the values are to 1, the better the station can simulate and represent rainfall for ungauged areas.

Discussion

As shown in Figs. 5, 6, 7, 8, and 9, the results of the events modeled by the WRF model, indicate that the Lin scheme provides for higher accuracy in rainfall modeling, concerning the observation data. This scheme can model the rainfall on the rain-gauge networks of 13–18 km in spacing in mountainous areas with an average FAR of 2.90 instances, while the corresponding figure to the gauge network in the plain area with a gauge spacing of 5–16 km was 2.60 instances. These results are in agreement with those reported by Coll-Hidalgo et al. (2020), Patel et al. (2019), and Zhu et al. (2021). The reason behind this concordance is that this scheme includes six classes of vapor-associated matters, including water cloud, water vapor, snow, rain, snow, and ice cloud, making it more reliable for arid areas like the one studied in this research. Moreover, the fact that this scheme (Lin) considers the collision of water particles upon precipitation in plain and mountainous areas make it different from the other schemes.

This difference then builds into the accuracy of Lin for rainfall forecast in the study area (Mohammadi et al. 2017). The verification analysis of the rain-gauge network across different parts of the study area indicates that the modeling results are generally more accurate and precise in plain areas, concerning the observation data. For instance, considering the Lin scheme, which was herein found to be the best option for rainfall forecast, networks in the mountainous areas ended up with TS and FAR levels of 0.83% and 0.17%, respectively, while the same scheme performed much better in the plain areas, as indicated by TS and FAR levels of 0.90% and 0.91%, respectively

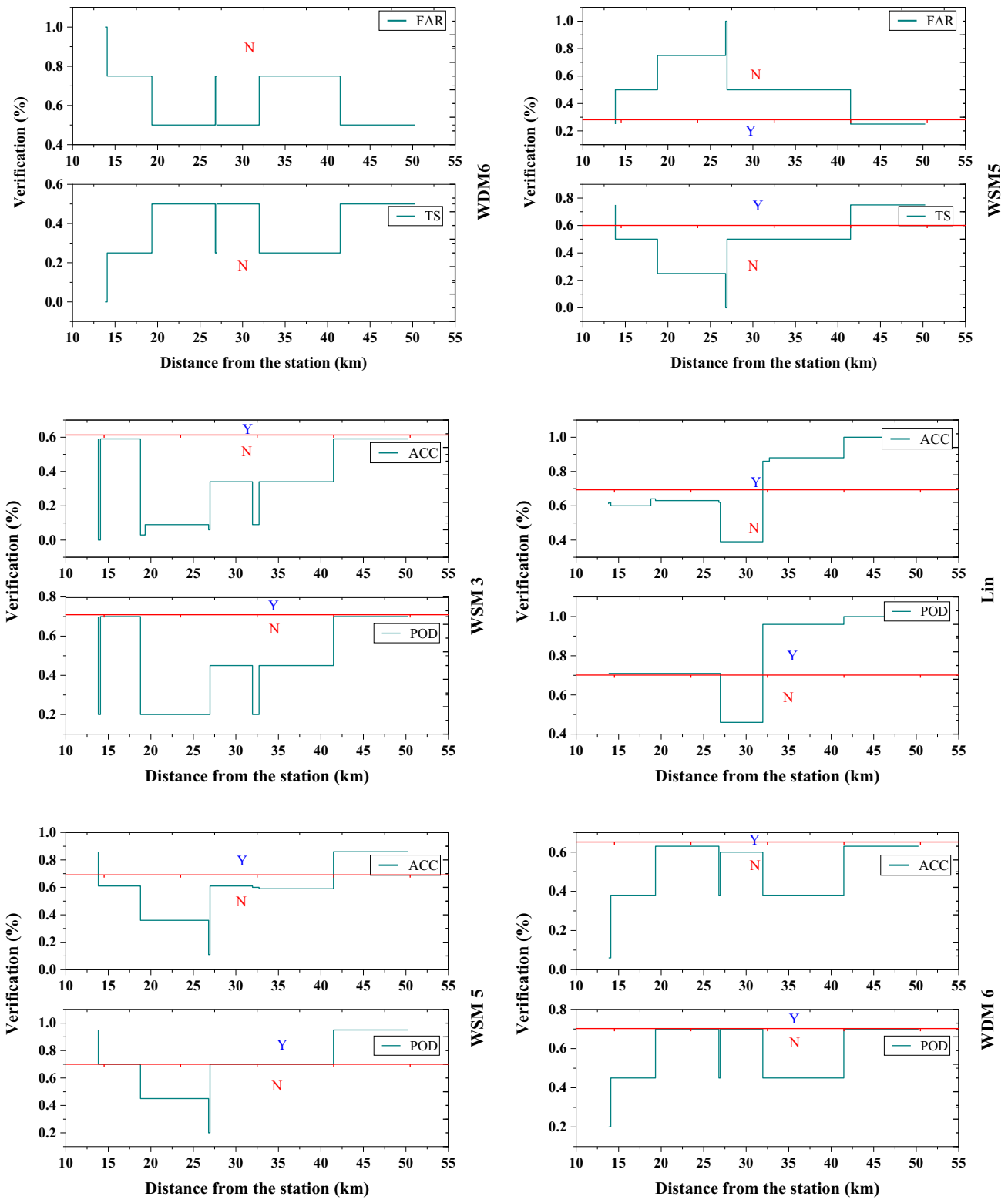

Fig. 7 (continued)

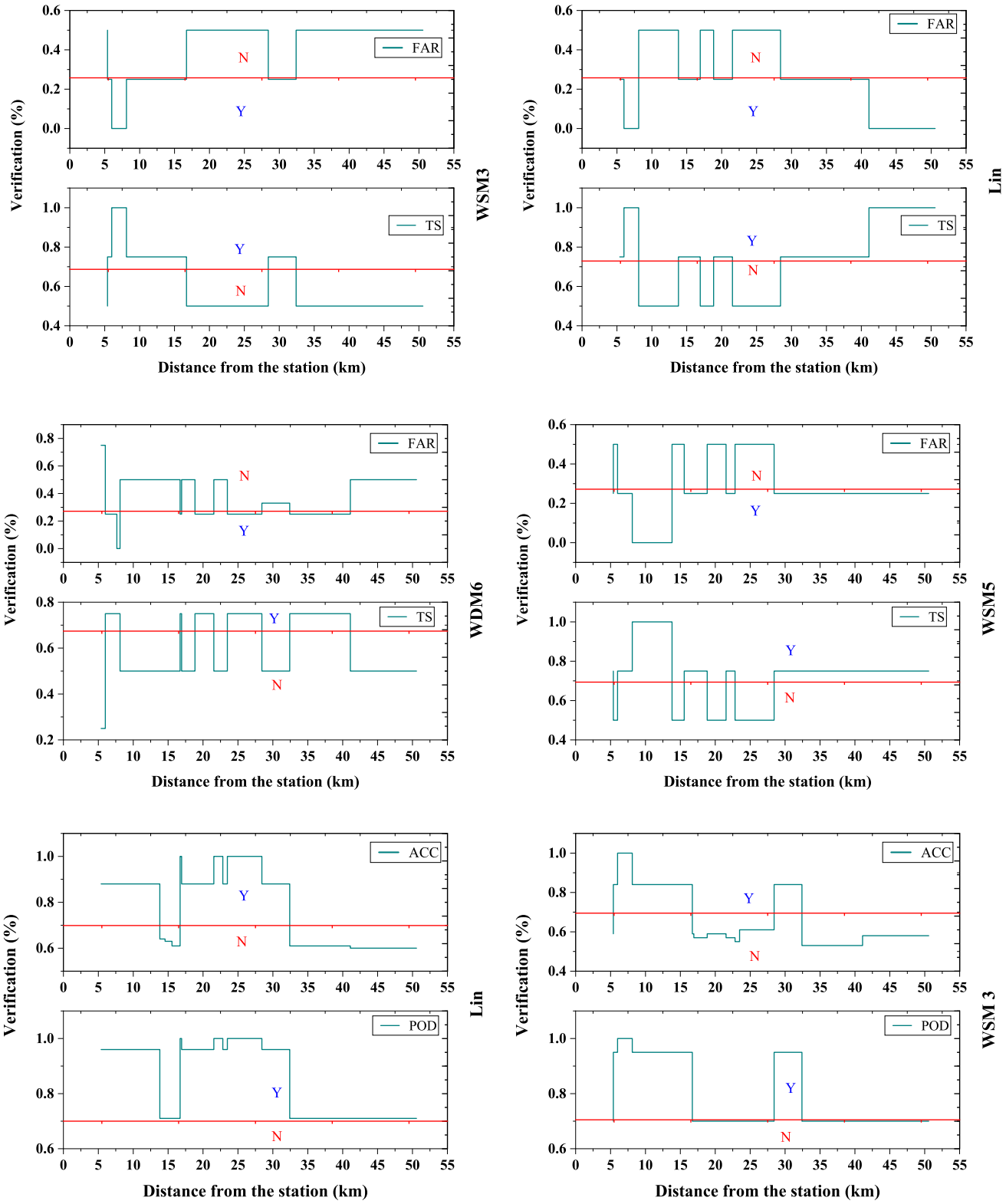

Fig. 8 Comparison of verification of different schemes in the network of rain gauge stations located in plains areas (Y: Acceptable, N: Unacceptable)

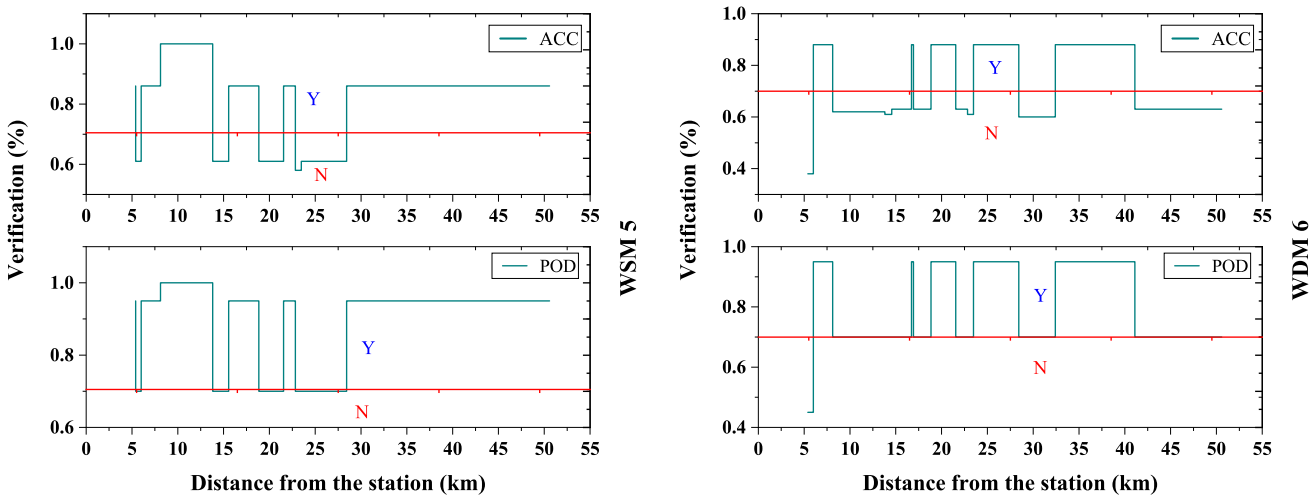

Fig. 8 (continued)

Table 7 Prediction of the best meteorological model scheme with the network of stations

Type of stations	No	Network of stations (km)	TS
Mountainous	1	13.82	1
	2	14.07	0.75
	3	18.78	0.75
	4	19.33	0.5
	5	26.79	0.5
	6	26.96	0.25
	7	31.95	0.75
	8	32.73	0.5
	9	41.48	0.75
	10	50.26	0.75
Plain	1	5.4	0.75
	2	6	0.75
	3	7.66	1
	4	8.11	1
	5	13.81	0.5
	6	14.56	0.75
	7	15.55	0.75
	8	16.72	0.75
	9	16.93	0.75
	10	18.85	0.5
	11	21.55	0.75
	12	22.83	0.5
	13	23.48	0.5
	14	28.43	0.5
	15	32.42	0.75
	16	41.1	0.75
	17	50.58	1

(Tables 8 and 9). This indicates a better accuracy of the WRF model than the remote sensing data. These results are consistent with those of Xu et al. (2017) who evaluated two rainfall events using TRMM and GPM satellites.

Based on previous studies Xu et al. (2021), these two satellite products outperformed other competitors at all spatial scales, as indicated by FARs of 21% and 14% for the TRMM and GPM, respectively. These levels of FAR suggested a higher accuracy than that of the WRF model in mountainous areas (Fig. 9). The results of this figure show that the output station of the WRF model at different distances from the Sabzevar synoptic station has better accuracy in several events. For example, in the Lin scheme, mountainous areas at a distance of 13 and 18 to 19 km have better accuracy in 3 events. This is while for plain areas at a distance of 4 to 30 km, have better accuracy in nearly 3 to 4 events.

A comparison between the results of the present research and those reported by (Xu et al. 2017) shows that the WRF model offers higher reliability levels for plain areas, where the TRMM and GPM data lead to FARs of 0.38 and 0.27%, respectively. These FARs are much higher than the outputs of the WRF model in plain areas. In contrast to other research works (Faraji et al. 2014; Gyasi-Agyei 2020), the present research eliminated the need for adding or omitting rain-gauge stations in areas where flood occurrence awareness/alarm and modeling are demanded, and the proposed rain-gauge network can be distributed in mountainous and plain areas with proper temporal and spatial resolutions. Despite this spatial distribution, one may design a network of acceptable accuracy for areas where adequate rain-gauge stations are not present or establishment of such rain-gauge stations is challenging.

By investigating the research findings, it was figured out that the dynamic meteorological model of WRF offers reliable levels of rainfall modeling and forecast accuracy even

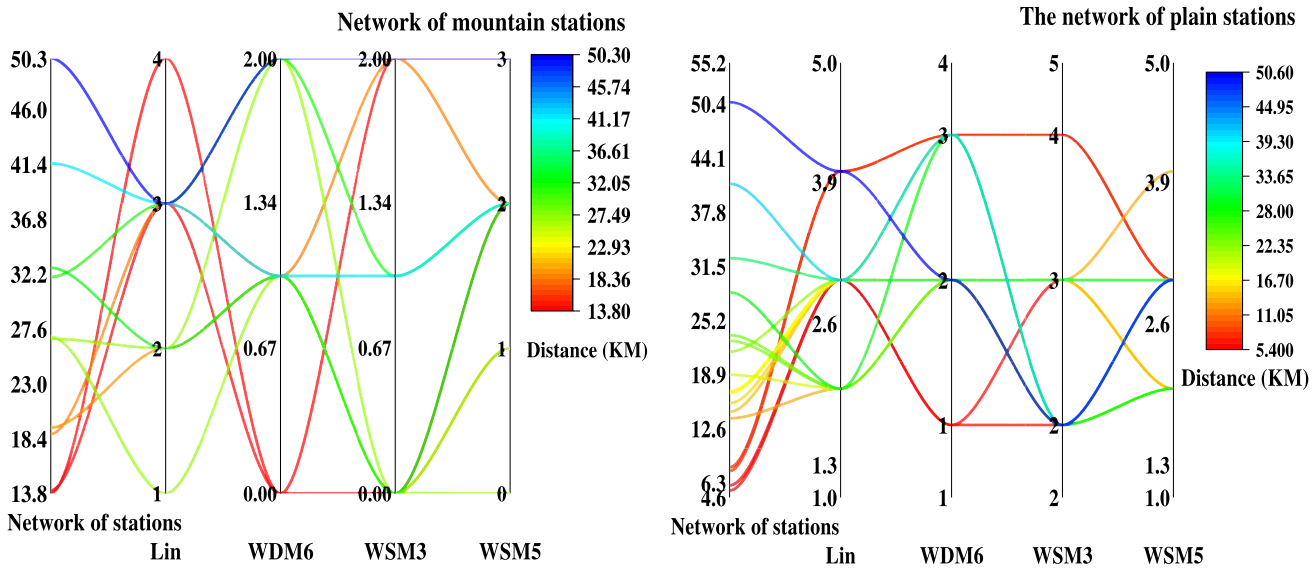

Fig. 9 False Alarm Ratio (FAR) in the network of the mountain and plain rain gauge stations

Table 8 Verification of the network of rain gauge stations in plain areas

Schemes	TS (%)	FAR (%)
Lin	91	09
WSM3	64	36
WSM5	67	33
WDM6	55	45

Table 9 Verification of the network of rain gauge stations in mountainous areas

Schemes	TS (%)	FAR (%)
Lin	83	17
WSM3	20	80
WSM5	45	55
WDM6	27	72

with other schemes, and this reliability is applicable when it is used for rainfall alarming in watersheds – that is, when the output of the WRF meteorological model is used to alarm a rainfall event qualitatively (e.g., a rainfall will/will not occur in the camping 24 h), which agrees well with the results of Pennelly et al. (2014) and Wu et al. (2019).

By reviewing the previous studies, it was found that the output of the WRF model can be used for all areas (plains and mountains). One of the innovations and advantages of this research is the forecast of rainfall for places without stations. With this method, in addition to the amount of rainfall, it is forecasted. Rain gauge stations Rain forecasting stations are established for places that are difficult to pass and difficult to access. The establishment of a rainfall forecasting station provides planners and experts in different areas of meteorology and hydrology a lot of help in estimating rainfall for flood warnings or input to hydrological models. Also, one of the most important innovations of this work, compared to previous research, is the creation of a virtual or spatial meteorological station for mountainous and plain areas at the same time. This study will help a lot for the regions of the world where the construction of the station is economically difficult.

Conclusion

Considering the devastating impacts of flood events, which have caused significant fatalities and financial losses over recent decades, human societies urgently require effective managerial solutions to mitigate flood-induced damages. One critical approach involves utilizing reliable future meteorological data (e.g., rainfall amounts) as input for hydrological modeling. The availability of such dependable data for future periods is essential for all countries worldwide. In this study, the WRF model was employed to simulate extreme rainfall events in arid regions of eastern Iran. The modeling results demonstrated that the Lin microphysical scheme provides the highest accuracy for rainfall modeling within the studied watershed. When applied to the rain-gauge network in both plain and mountainous areas, this scheme achieved Threat Scores (TS) of 0.91 and 0.83, respectively, indicating superior performance in plain regions. Further investigations revealed that this scheme effectively modeled extreme rainfall events in the study area, as evidenced by its zero deviation from observed data at specific stations. Based on these findings, it is recommended to adopt the Lin scheme for predicting rainfall in future 24-hour periods. Such forecasts can

be integrated with existing rain-gauge networks to extend coverage to non-gauged areas, thereby enhancing the input data for hydrological models. Additionally, designing a rain-gauge network based on this approach can facilitate early warning systems for areas without terrestrial stations, enabling proactive measures to address potential crises. The outcomes of this research provide valuable insights for water resource managers, flood mitigation planners, and crisis management officials, helping them anticipate future flood events and implement strategies to minimize environmental, socioeconomic, and other related damages.

Acknowledgements We would like to thank the Iranian Meteorological Organization (IRIMO) for providing the observational data of the study area. The authors are also grateful to the Research Institute of Meteorology and Atmospheric Sciences (RIMAS) for its scientific support of the present study.

Author contributions All authors contributed to the study's conception and design. Material preparation, data collection, and analysis were performed by Mahdi Zarei, Rasoul Sarvestan and Seyed Hassan Alavinia. The first draft of the manuscript was written by Rasoul Sarvestan and all authors carried out editing and writing and commented on previous versions of the manuscript. All authors read and approved the final manuscript.

Funding The authors received no financial support for the research, authorship, and/or publication of this article.

Data availability The observational rainfall data is from the Iran Meteorological Organization https://www.irimo.ir/eng/index.php. The Global Forecast System (GFS) datasets for this research were obtained from https://www.ncei.noaa.gov/data/global-forecast-system/access/historical/forecast/grid-004-0.5-degree/.

Declarations

Competing interests The authors declare no competing interests.

References

Adhikary SK, Yilmaz AG, Muttil N (2015) Optimal design of rain gauge network in the Middle Yarra River catchment, Australia. Hydrol Process 29(11):2582–2599

Astin I (1997) A survey of studies into errors in large scale space-time averages of rainfall, cloud cover, sea surface processes and the earth's radiation budget as derived from low earth orbit satellite instruments because of their incomplete temporal and spatial coverage. Surv Geophys 18(4):385–403

Ayanwale OA, Alabi O (2017) Ground validation of GPM IMERG and TRMM 3B42V7 rainfall products over Nigerian eLightning. Paper presented at the AGU Fall Meeting 2019

Bae SY, Hong S-Y, Lim K-SS (2016) Coupling WRF double-moment 6-class microphysics schemes to RRTMG radiation scheme in weather research forecasting model. Adv Meteorol 2016

Bastin G, Lorent B, Duque C, Gevers M (1984) Optimal estimation of the average areal rainfall and optimal selection of rain gauge locations. Water Resour Res 20(4):463–470

Castorina G, Caccamo MT, Insinga V, Magazù S, Munaò G, Ortega C, Rizza U (2022) Impact of the differe grid resolutions of the WRF model for the forecasting of the flood event of 15 July 2020 in Palermo (Italy Atmosphere. 13(10):1717

Chua S-H, Bras RL (1982) Optimal estimators of mean areal precipitation in regions of orographic influence. J Hydrol 57(1–2):23–48

Coll-Hidalgo P, Pérez-Alarcón A, González-Jardines P (2020) Evaluation of microphysics schemes in the WRF-ARW model for numerical wind forecast in José Martí International Airport. Paper presented at the Environmental Sciences Proceedings

Coustau M, Rousset-Regimbeau F, Thirel G, Habets F, Janet B, Martin E, Soubeyroux J-M (2015) Impact of improved meteorological forcing, profile of soil hydraulic conductivity and data assimilation on an operational Hydrological Ensemble Forecast System over France. J Hydrol 525:781–792

Das MK, Islam AS, Karmakar S, Khan JU, Mohammed K, Islam GT, Bala SK (2020) Investigation of Flash Flood producing rainstorm in Northeast Bangladesh using WRF model. Water, Flood Management and Water Security under a changing climate. Springer, pp 163–175

Davis S, Pentakota L, Saptarishy N, Mujumdar P (2022) A flood forecasting framework coupling a hi resolution WRF ensemble with an urban hydrologic model. Front Earth Sci 10:883842

Faraji H, Meymand M, Nazif S, Abbaspour R (2014) Optimal development of rain gauge network using kriging and entropy methods in GIS environment (case study: Karkheh catchment). Nat Geogr Res 46(4):445–462

Fortin G, Acquaotta F, Fratianni S (2017) The evolution of temperature extremes in the Gaspé Peninsula, Quebec, Canada (1974–2013). Theoret Appl Climatol 130(1):163–172

Gyasi-Agyei Y (2020) Identification of the optimum rain gauge network density for hydrological modelling based on radar rainfall analysis. Water 12(7):1906

Habets F, Boone A, Champeaux JL, Etchevers P, Franchistéguy L, Leblois E, Noilhan J, Quintana Segui F, Rousset-Regimbeau P, Viennot P (2008) The SAFRAN-ISBA-MODCOU hydrometeorological model applied over France. J Geophys Res 113:D06113. https://doi.org/10.1029/2007JD008548

Hong S-Y, Lim J-OJ (2006) The WRF single-moment 6-class microphysics scheme (WSM6). Asia-Pac J Atmos Sci 42(2):129–151

Hong S-Y, Dudhia J, Chen S-H (2004) A revised approach to ice microphysical processes for the bulk parameterization of clouds and precipitation. Mon Weather Rev 132(1):103–120

Hong Y, Gochis D, Cheng J-t, Hsu K-l, Sorooshian S (2007) Evaluation of PERSIANN-CCS rainfall measurement using the NAME event rain gauge network. J Hydrometeorol 8(3):469–482

Hou S (2018) How does the evaluation of GPM IMERG rainfall product depend on gauge density and rainfall intensity? Paper presented at the AGU Fall Meeting Abstracts

Jung Y, Kim H, Baik J, Choi M (2014) Rain-gauge network evaluations using spatiotemporal correlation structure for semi-mountainous regions. TAO: Terr Atmospheric Ocean Sci 25(2):267

Kain JS (2004) The Kain–Fritsch convective parameterization: an update. J Appl Meteorol 43(1):170–181

Kodamana R, Fletcher CG (2021) Validation of CloudSat-CPR Derived Precipitation occurrence and phase estimates across Canada. Atmosphere 12(3):295

Krajewski W, Smith JA (2002) Radar hydrology: rainfall estimation. Adv Water Resour 25(8–12):1387–1394

Kreklow J, Tetzlaff B, Kuhnt G, Burkhard B (2019) A rainfall data intercomparison dataset of RADKLIM, RADOLAN, and rain gauge data for Germany. Data 4(3):118

Kuznetsova A, Baydakov G, Sergeev D, Troitskaya Y (2019) High–resolution waves and weather forecasts using adapted

WAVEWATCH III and WRF models. Paper presented at the Journal of Physics: Conference Series
Lim K-SS, Hong S-Y (2010) Development of an effective double-moment cloud microphysics scheme with prognostic cloud condensation nuclei (CCN) for weather and climate models. Mon Weather Rev 138(5):1587–1612
Lin C-Y, Chen W-C, Liu SC, Liou YA, Liu G, Lin T (2008) Numerical study of the impact of urbanization on the precipitation over Taiwan. Atmos Environ 42(13):2934–2947
Lin C-Y, Chen W-C, Chang P-L, Sheng Y-F (2011) Impact of the urban heat island effect on precipitation over a complex geographic environment in northern Taiwan. J Appl Meteorol Climatology 50(2):339–353
Liu C, Ikeda K, Thompson G, Rasmussen R, Dudhia J (2011) High-resolution simulations of wintertime precipitation in the Colorado headwaters region: sensitivity to physics parameterizations. Mon Weather Rev 139(11):3533–3553
Maddox RA, Zhang J, Gourley JJ, Howard KW (2002) Weather radar coverage over the contiguous United States. Weather Forecast 17(4):927–934
Mafas M, Muhammadh K, Weerakoon S, Mutua F (2016) Comparative study of WRF and REGCM weather predictions for the Upper Mahaweli River Basin. Paper presented at the Proceedings of the 7th International Conference on Sustainable Built Environment, Kandy, Sri Lanka
Mahoutchi MH, Abbasi E (2021) Assessment of WRF model sensitivity for simulating super heavy precipitation. J Water Soil Conserv 28(1):45–66
Merino A, García-Ortega E, Navarro A, Fernández-González S, Tapiador FJ, Sánchez JL (2021) Evaluation of gridded rain-gauge-based precipitation datasets: impact of station density, spatial resolution, altitude gradient and climate. Int J Climatol 41(5):3027–3043
Mohammadi H, Azizi G, Khoshahklagh F, Ranjbar F (2017) Analysis of daily precipitation extreme indices trend in Iran. Phys Geogr Res Q 49(1):21–37
Mohammadiha A, Memarian M, Azadi M, Parvari R (2012) Verification of WRF Model forecatings for content of precipitable water and precipitation with the RADAR data. Thesis submitted For the degree of M.Sc, 1-160
Morin E, Goodrich DC, Maddox RA, Gao X, Gupta HV, Sorooshian S (2006) Spatial patterns in thunderstorm rainfall events and their coupling with watershed hydrological response. Adv Water Resour 29(6):843–860
Morsy M, Taghizadeh-Mehrjardi R, Michaelides S, Scholten T, Dietrich P, Schmidt K (2021) Optimization of rain gauge networks for arid regions based on remote Sensing Data. Remote Sens 13(21):4243
Naing SM (2021) Sensitivity analysis of heavy rainfall events on physical parameterization configurations using. WRF-ARW Model over Myanmar, pp 1–125
NCEP G (2015) 0.25 Degree global forecast grids historical archive (Research data archive at the national center for atmospheric research, computational and information systems laboratory. National centers for environmental prediction/national weather service/NOAA/US Department of Commerce. Boulder, CO
Patel P, Ghosh S, Kaginalkar A, Islam S, Karmakar S (2019) Performance evaluation of WRF for extreme flood forecasts in a coastal urban environment. Atmos Res 223:39–48
Pennelly C, Reuter G, Flesch T (2014) Verification of the WRF model for simulating heavy precipitation in Alberta. Atmos Res 135:172–192
Putthividhya A, Tanaka K (2012) Optimal rain gauge network design and spatial precipitation mapping based on geostatistical analysis from colocated elevation and humidity data. Int J Environ Sci Dev 3(2):124
Rahman MS (2017) Effect of differently interpolated Geographical Data on WRF-ARW Forecast. Khulna University of Engineering & Technology (KUET), Khulna, Bangladesh
Raimonet M, Oudin L, Thieu V, Silvestre M, Vautard R, Rabouille C, Le Moigne P (2017) Evaluation of gridded meteorological datasets for hydrological modeling. J Hydrometeorol 18(11):3027–3041
Rodrigo C, Kim S, Jung IH (2018) Sensitivity study of WRF numerical modeling for forecasting heavy rainfall in Sri Lanka. Atmosphere 9(10):378
Sarvestan R, Karami M, Sabbaghian RJ (2022) Assessment of the weather research and forecasting model in simulation of rainfall for Khorasan Razavi Province, Iran. Arab J Geosci 15(2):164
Satya O, Kaban H, Irfan M, Rahmasari K, Monica C, Sari D, Mandahiling P (2021) Evaluation of several cumulus parameterization schemes for daily rainfall predictions over Palembang City. Paper presented at the Journal of Physics: Conference Series
Shafiei M, Ghahraman B, Saghafian B, Pande S, Gharari S, Davary K (2014) Assessment of rain-gauge networks using a probabilistic GIS based approach. Hydrol Res 45(4–5):551–562
Skamarock WC, Klemp JB, Dudhia J, Gill DO, Barker DM, Duda MG, Powers JG (2008) A description of the advanced research WRF version 3. NCAR technical note 475(125):10–5065
Smith JA, Seo DJ, Baeck ML, Hudlow MD (1996) An intercomparison study of NEXRAD precipitation estimates. Water Resour Res 32(7):2035–2045
Soci C, Bazile E, Besson F, Landelius T (2016) High-resolution precipitation re-analysis system for climatological purposes. Tellus A: Dynamic Meteorol Oceanogr 68(1):29879
Statistical Center of Iran (2019) Statistical yearbook, land and climate. pp 115–125
Tian F, Hou S, Yang L, Hu H, Hou A (2018) How does the evaluation of the GPM IMERG rainfall product depend on gauge density and rainfall intensity? J Hydrometeorol 19(2):339–349
Tiwari S, Jha Sk, Singh A (2020) Quantification of node importance in rain gauge network: influence of temporal resolution and rain gauge density. Sci Rep 10(1):1–17
Usowicz B, Lipiec J, Łukowski M, Słomiński J (2021) Improvement of spatial interpolation of precipitation distribution using cokriging incorporating rain-gauge and satellite (SMOS) soil moisture data. Remote Sens 13(5):1039
Verlinde J, Flatau PJ, Cotton WR (1990) Analytical solutions to the collection growth equation: comparison with approximate methods and application to cloud microphysics parameterization schemes. J Atmos Sci 47(24):2871–2880
Villarini G, Mandapaka PV, Krajewski WF, Moore RJ (2008) Rainfall and sampling uncertainties: a rain gauge perspective. J Geophys Research: Atmos 113:D11
Volkmann TH, Lyon SW, Gupta HV, Troch PA (2010) Multicriteria design of rain gauge networks for flash flood prediction in semiarid catchments with complex terrain. Water Resour Res 46(11)
Wu T, Min J, Wu S (2019) A comparison of the rainfall forecasting skills of the WRF ensemble forecasting system using SPCPT and other cumulus parameterization error representation schemes. Atmos Res 218:160–175
Xu R, Tian F, Yang L, Hu H, Lu H, Hou A (2017) Ground validation of GPM IMERG and TRMM 3B42V7 rainfall products over southern Tibetan Plateau based on a high-density rain gauge network. J Geophys Research: Atmos 122(2):910–924
Xu W, Liu P, Cheng L, Zhou Y, Xia Q, Gong Y, Liu Y (2021) Multi-step wind speed prediction by combining a WRF simulation and an error correction strategy. Renewable Energy 163:772–782
Yatheendradas S, Wagener T, Gupta H, Unkrich C, Goodrich D, Schaffner M, Stewart A (2008) Understanding uncertainty in distributed flash flood forecasting for semiarid regions. Water Resour Res 44(5)
Young CB, Nelson BR, Bradley AA, Smith JA, Peters-Lidard CD, Kruger A, Baeck ML (1999) An evaluation of NEXRAD precipitation estimates in complex terrain. J Geophys Research: Atmos 104(D16):19691–19703

Yue H, Gebremichael M, Nourani V (2022) Evaluation of global Forecast System (GFS) medium-range precipitation forecasts in the Nile River Basin. J Hydrometeorol 23(1):101–116

Zhang X, Yang F (2004) RClimDex 1.0 user manual. Climate Research Branch Environment Canada, 22:13–14

Zhu J, Zhang S, Yang Q, Shen Q, Zhuo L, Dai Q (2021) Comparison of rainfall microphysics characteristics derived by numerical weather prediction modelling and dual-frequency precipitation radar. Meteorol Appl 28(3):e2000